Multi-photon UV photolysis of gaseous polycyclic aromatic hydrocarbons: Extinction spectra and dynamics

Cite as: J. Chem. Phys. **139**, 054304 (2013); https://doi.org/10.1063/1.4816003
Submitted: 07 March 2013 . Accepted: 04 July 2013 . Published Online: 05 August 2013

A. J. Walsh, A. A. Ruth, E. W. Gash, and M. W. D. Mansfield

Multi-photon UV photolysis of gaseous polycyclic aromatic hydrocarbons: Extinction spectra and dynamics

A. J. Walsh,[1,a)] A. A. Ruth,[1,2,b)] E. W. Gash,[1] and M. W. D. Mansfield[1]
[1]*Physics Department, University College Cork, Cork, Ireland*
[2]*Environmental Research Institute, University College Cork, Cork, Ireland*

(Received 7 March 2013; accepted 4 July 2013; published online 5 August 2013)

The extinction spectra of static naphthalene and static biphenylene vapor, each buffered with a noble gas at room temperature, were measured as a function of time in the region between 390 and 850 nm after UV multi-photon laser photolysis at 308 nm. Employing incoherent broadband cavity enhanced absorption spectroscopy (IBBCEAS), the spectra were found to be unstructured with a general lack of isolated features suggesting that the extinction was not solely based on absorption but was in fact dominated by scattering from particles formed in the photolysis of the respective polycyclic aromatic hydrocarbon. Following UV multi-photon photolysis, the extinction dynamics of the static (unstirred) closed gas-phase system exhibits extraordinary quasi-periodic and complex oscillations with periods ranging from seconds to many minutes, persisting for up to several hours. Depending on buffer gas type and pressure, several types of dynamical responses could be generated (classified as types I, II, and III). They were studied as a function of temperature and chamber volume for different experimental conditions and possible explanations for the oscillations are discussed. A conclusive model for the observed phenomena has not been established. However, a number of *key hypotheses* have made based on the measurements in this publication: (a) Following the multi-photon UV photolysis of naphthalene (or biphenylene), particles are formed on a timescale not observable using IBBCEAS. (b) The observed temporal behavior cannot be described on basis of a chemical reaction scheme alone. (c) The pressure dependence of the system's responses is due to transport phenomena of particles in the chamber. (d) The size distribution and the refractive indices of particles are time dependent and evolve on a timescale of minutes to hours. The rate of particle coagulation, involving coalescent growth and particle agglomeration, affects the observed oscillations. (e) The walls of the chamber act as a sink. The wall conditions (which could not be quantitatively characterized) have a profound influence on the dynamics of the system and on its slow return to an equilibrium state.
 [http://dx.doi.org/10.1063/1.4816003]

I. INTRODUCTION

Polycyclic aromatic hydrocarbons (PAHs) and their cationic forms are involved in a significant part of the chemistry governing the natural environment as well as the interstellar medium (i.e., the matter that exists in the space between star systems). The combination of the mutagenic and/or carcinogenic properties of many PAHs[1,2] and their efficient formation during the incomplete combustion of organic materials, has resulted in a large effort to understand the fundamental role of PAHs in combustion chemistry.[3,4] Hence, their physical and chemical properties have been extensively studied under a variety of environmentally relevant experimental conditions, e.g., in shock-tube pyrolysis[5,6] and flame combustion studies.[7,8] Due to their strong affinities to carbonaceous matter, such as coal or soot, the occurrence of PAHs in fine particulate matter in the atmosphere and their formation, e.g., in the context of black carbon particles,[9] is of significant interest in atmospheric/environmental sciences.[10,11] Gaseous (monomeric) PAHs (notably naphthalene[10]) are an important class of tropospheric pollutant, whose role for the generation of secondary organic aerosol has also been recently addressed.[12]

In the context of astrochemistry, PAHs are thought to be ubiquitous in the interstellar medium since they carry the infrared emission features that dominate the spectra of most galactic and extragalactic sources.[13] The absorption of PAH ions in the visible has made them prime candidates as potential carriers of the diffuse interstellar bands,[14–16] a series of broad absorption lines in the visible; they are also potentially causing the omnipresent emission bands in the 3.3–11 μm region.[17,18]

In the present work, the UV photolysis products of static room temperature gaseous PAHs, buffered with a noble gas, were studied by measuring their wavelength-dependent extinction between 390 and 850 nm, using incoherent broadband cavity enhanced absorption spectroscopy (IBBCEAS).[19,20] The photolysis products were found to cause strong optical losses in this region, with complex time-dependence, ranging from simple growth/decay dynamics, via quasi-oscillatory to more complex time-dependent behavior. The time-dependent behavior of the extinction of naphthalene–buffer gas mixtures after UV photolysis represents an intriguing new observation that has not been investigated systematically before.

[a)]Present address: Sackler Laboratory for Astrophysics, Leiden Observatory, University of Leiden, The Netherlands.
[b)]Author to whom correspondence should be addressed. Electronic mail: a.ruth@ucc.ie.

This gas-phase system exhibits oscillatory behavior with periods on a timescale of many minutes, while being initiated on a timescale of nanoseconds. In the past systems, exhibiting oscillatory dynamics have largely been based on chemical reaction mechanisms in the condensed phase.[21] Oscillations in the gas-phase are, to the best of our knowledge, only known for flow reactors and combustion chambers with spontaneous oxidations of small compounds.[22,23] In Ref. 24, we published initial results and observations of this unusual gas-phase system. The work presented here is the continuation of this investigation, therefore, the most important experimental findings of Ref. 24 are briefly summarized in the following.

The system consisted of gaseous naphthalene buffered with a noble gas in a static gas chamber at room temperature. The unstirred gas mixture was exposed to a small number of strong, focused UV laser pulses (at 308 nm, 15 ns duration), leading to resonance-enhanced multi-photon ionization and fragmentation of naphthalene. Immediately after this photolysis, the extinction of the photoproducts generated in the chamber was measured as a function of time at 650 nm, using the sensitive cavity ring-down (CRD) absorption method[25] (note: at 650 nm neutral naphthalene is completely transparent, the observed extinction was solely due to the unknown photoproducts formed during the photolysis; the potential absorption of the naphthalene cation will be discussed in Sec. VI A). The time-dependence of the extinction was found to be strongly dependent on the specific experimental conditions. Depending on the type of buffer gas and its partial pressure (He between 5 and 120 mbar, Ar between 4 and 30 mbar) as well as the number and energy of the UV pulses used in the multi-photon photolysis, three types of temporal extinction responses could be distinguished:[24,26]

Type I. *Simple growth and decay:* At "low" partial pressures of the buffer gas, fast growth-decay behavior in the extinction was observed with typical durations of 5–25 s (FWHM). The term *low* partial pressure refers to the range of ∼5–∼70 mbar in He and ∼5–∼7.5 mbar in Ar. This type of temporal extinction response of the system is most reproducible; the reproducibility is subject to the degradation of the initial gas mixture. An example of growth and subsequent decay at low pressures is shown in Figure 1(a).[26]

Type II. *Quasi-periodic oscillations with one or more components:* At "medium" partial pressures of the buffer gas, oscillations in the extinction of the photolysis products are observed with long periods ranging from many seconds up to many minutes. The oscillatory behavior can persist for several hours (Figure 1(b)). The term *medium* partial pressure refers to the range of ∼70 to ∼80 mbar in He and ∼7.5 to ∼12 mbar in Ar. The extinction during oscillations can be an order of magnitude larger than in simple growth/decay responses (type I); amplitudes can be as large as $\Delta\alpha \sim 3\times10^{-5}$ cm^{-1}. The oscillatory response often consists of more than one independently varying component.

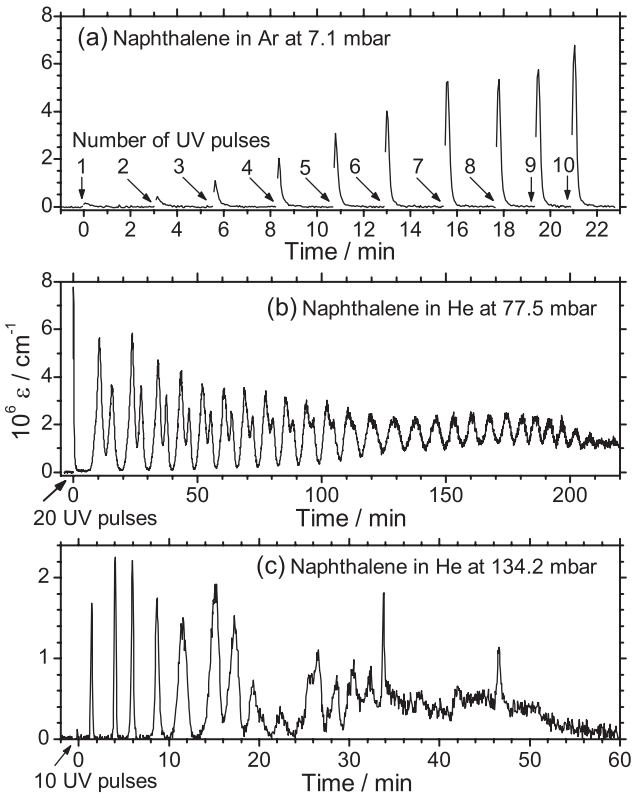

FIG. 1. Extinction coefficient at 650 nm as a function of time. (a) Example of type I dynamic behavior. Arrows indicate the excitation of the gas mixtures with n (=1…10) focused UV pulses. $E_{pulse} \sim 24$ mJ. (b) Example of type II dynamic behavior. The arrow indicates the time of excitation with 20 focused UV pulses; $E_{pulse} \sim 18$ mJ. (c) Example of type III dynamic behavior. The arrow indicates the time of excitation with 10 focused UV pulses. $E_{pulse} \sim 10$ mJ. Respective buffer gases and pressures are stated in the panel. UV repetition rate 10 Hz.

Type III. *Complex dynamic behavior:* At "high" partial pressures of the buffer gas, and on certain occasions also at pressures which were categorized as "medium," complex temporal responses were observed (an example is shown in Figure 1(c)).

Quasi-periodic oscillations and complex temporal responses (types II and III) are strongly dependent on all relevant experimental parameters and are only reproducible qualitatively, i.e., amplitudes (and also periods in case of type II) can vary significantly from measurement to measurement.[24] There is, however, no evidence yet that chaotic properties can be attributed to the system. Under several experimental conditions, *no extinction* was observed after multi-photon UV excitation:

(1) When the UV laser beam was not focused.
(2) With only the buffer gas present in the chamber – helium or argon (no naphthalene vapor).
(3) With only naphthalene present in the cell (no buffer gas).
(4) Stirring of the gas mixture with a fan (the effect of stirring the gas mixture will be further discussed in Sec. VI C 3).

Additionally, it was established that for conditions when the system was continuously exposed to UV pulses, a slow but continuous increase of extinction was observed, followed by

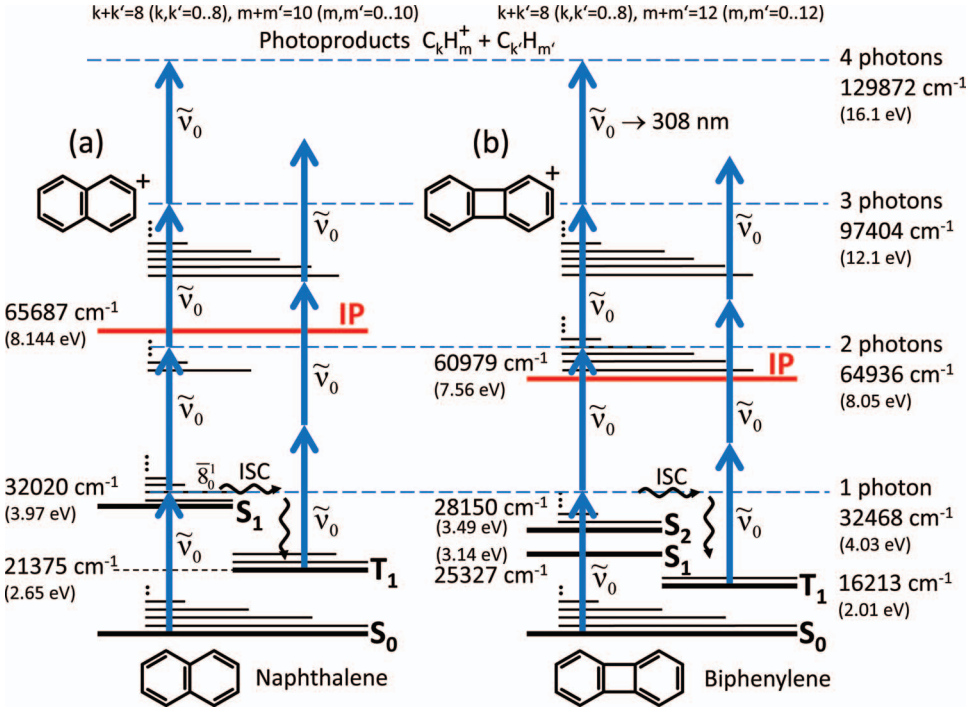

FIG. 2. Resonance-enhanced n-photon absorption processes of (a) naphthalene (left) and (b) biphenylene (right) upon excitation at $\tilde{\nu}_0 = 32\,468$ cm^{-1} (308 nm), illustrated in two schematic Jabłoński diagrams. The energies of the 1- to 4-photon processes in the singlet manifold are indicated by horizontal dashed blue lines with the corresponding values on the right. IP = ionization potential.

strong oscillatory behavior only when the UV irradiation was stopped (see Sec. SII in the supplementary material).[27] This observation shows that the UV radiation inhibits the mechanisms that enable the occurrence of oscillatory extinction behavior, probably by preventing the formation of relevant types of photoproducts or other essential components. The most striking feature of this gas-phase system is the remarkably long time that it is able to remain away from an equilibrium state. The time scale on which it evolves appears unique for a gas-phase system. No experimental results, which can be directly compared with the presented data, could be found in the literature.

Naphthalene and also biphenylene are the target molecules of this study. Thus, in Sec. II, we will briefly review the photophysics and photo-fragmentation of naphthalene and biphenylene as far as this is relevant for the excitation process. The experimental cavity enhanced absorption setup will be described in Sec. III. In Secs. IV and V, new results on the time-dependent extinction spectra of the multi-photon UV photolysis products of naphthalene- and biphenylene noble gas mixtures will be outlined, respectively. We will then present a discussion in Sec. VI concerning the interpretation of the results based on the considerations what species are formed in the photolysis. Additional information will be presented in support of a hypothesis that carbonaceous particles are generated upon multi-photon excitation (note: the description of spectra by a Mie scattering model in the context of particle formation will be the subject of future work (unpublished)[28]). The experimental parameters governing the system's temporal response will then be discussed (Secs. VI C and VI D) based on some additional observations and general features characterizing the dynamics of the system.

II. PHOTOPHYSICS OF NAPHTHALENE AND BIPHENYLENE

A. Naphthalene

Naphthalene (C_8H_{10}) is an extensively studied polycyclic aromatic hydrocarbon with a singlet electronic ground state, S_0. Upon exposure to high UV photon fluences, naphthalene will undergo a resonance-enhanced n-photon absorption process ($n \geq 1$)[29–32] as schematically shown in Figure 2(a). The first photon at $\tilde{\nu}_0 = 32\,468$ cm^{-1} (308 nm) is in resonance with a vibronic state $\bar{8}_0^1$, 438 cm^{-1} into the vibrational manifold of the first electronically excited singlet state S_1 at 32 020 cm^{-1}.[33] The vibronic state $S_{1,\nu}(\bar{8}_0^1)$ is known to have a lifetime of ~270 ns in the collision free limit.[34] The energy deactivation rate of the S_1 state of naphthalene in 70 mbar of helium is $\approx 3.8 \times 10^{-3}$ ns^{-1}. Direct absorption $S_{n,\nu'} \leftarrow S_{1,\nu}(\bar{8}_0^1)$ of a second photon brings the molecule very close to the well-known ionization threshold of (65 666 ± 5) cm^{-1} (=(8.141 ± 0.001) eV), which was determined, e.g., in a two-color photoionization experiment[29] using the same $S_{1,\nu}(\bar{8}_0^1)$ resonance as in the present case. Since the two-photon energy is only 730 cm^{-1} below the ionization threshold, ≈3% of hot naphthalene molecules at $T = 298$ K are ionized by this two-photon resonance-enhanced absorption process in the singlet manifold. Due to the high density of states $S_{n,\nu'}$ below the ionization threshold the absorption of a third photon is again resonance-enhanced promoting naphthalene well above the ionization potential (IP).

A fraction of the naphthalene can also be ionized via the triplet manifold (Sec. SI B in the supplementary material[27]). Experiments by Gattermann and Stockburger[35] suggest that in the vibrational S_1 manifold intersystem crossing (ISC)

is dominating the nonradiative relaxation. For the vibronic state $S_{1,\nu}(\bar{8}_0^1)$, quantum yields of prompt fluorescence and intersystem crossing were reported to be ≈0.36 and ≈0.64, respectively.[33]

To estimate the percentage of naphthalene molecules which undergo photolysis, via the singlet manifold, at the focus of the UV excitation beam, the excitation process of the naphthalene molecule was modelled on basis of a scheme, containing S_0, S_1, S_n, and the cationic electronic state D_m as well as five possible transitions. The assumptions used for this calculation and the results of time dependent populations of states involved in the model is outlined in detail in Figure S1 in the supplementary material.[27] Despite the fact that ionization through the triplet manifold was not explicitly considered, it was found that naphthalene cations were created efficiently at the focus of the UV pulse. Assuming a Gaussian laser beam in time and space with a beam waist $r < 50\ \mu$m at the focus ∼100% of molecules are photolyzed through the resonance-enhanced absorption of three photons. Thus, further excitation of the cation through absorption of a fourth photon leads to fragmentation. As the intramolecular dynamics and dissociation energies of $C_{10}H_8^+$ are similar to those of neutral $C_{10}H_8$,[35] from the estimated percentage of cations formed, the fragmentation probability of the naphthalene cation is large. The electron recombination rate for the $C_{10}H_8^+$ cation is $(8 \pm 2) \times 10^2$ cm^3 ns^{-1}.[36] The time between excitation pulses at the maximum laser repetition rate (50 Hz) used in this work was much longer than the recombination time, therefore, only neutral species were present for each UV photolysis pulse, which is confirmed by an estimate of a typical diffusion time of products away from photolysis zone (Sec. SV in the supplementary material).[27]

1. Fragmentation of naphthalene

The low lying electronic states of the naphthalene cation (D1 … D5), which are connected to the ionic ground state D_0 by π–π transitions have attracted much attention in the past[37–39] due to their relevance in absorption studies involving compounds which may potentially cause the so-called "diffuse interstellar bands" that are observed in the line of sight of many stars.[15,40,41]

The photodissociation of gas-phase naphthalene well above the ionization threshold has been extensively studied experimentally in the past,[42–44] using mass spectrometry in conjunction with a variety of ionization techniques such as electron-impact[45] and collision induced methods,[46] multi-photon photoionization in ion-traps[47–49] and in supersonic molecular jets,[50] and single-photon ionization in effusive beams using synchrotron radiation.[44,51,52] There are also a number of theoretical studies on that topic,[53–55] some of them considering subsequent reaction pathways with other neutral or ionized compounds[56,57] or in the context of nucleation reaction and soot formation, see Sec. VI B.

A variety of fragmentation channels at different activation energies (AE) have been established (listed in Table I), which can be divided into a group of low- and high-energy processes.[42] The unimolecular dissociations fall mainly into a "low energy" group, (AE < 16 eV) and a "high energy" group (AE > 18 eV). The reactions in the "low energy" group have the bicyclic precursor $C_{10}H_8^+$ in common, which decays via rupture of one ring. The "high energy" group reactions involve rupture of both rings to give an open chain precursor, the 1,6-bis-ethinyl-hexatriene radical cation. All of the low-energy dissociation channels, which dominate the fragmentation of naphthalene, are energetically possible upon 4-photon excitation (16.1 eV). Among the most prominent low-energy fragmentation pathways, the most important comprises –H (15.35 eV), $-H_2$ (15.6 eV), and $-C_2H_2$ loss reactions, which are considered in detail by Ref. 42. The appearance energy for the C_2H_2 channel was reported to be between 14.3 and 15.63 eV.[42,45,47,51] In Ref. 48, the complete photodestruction of the naphthalene cation is reported, which is suggested to proceed via subsequent C_2H_2 loss: $C_{10}H_8^+ + h\nu \rightarrow C_{10}H_8^+ - n\,(C_2H_2)$ with $(n = 1 \ldots 4)$.

TABLE I. Summary of appearance energies of naphthalene fragments.

Cationic product	Neutral product	Average appearance energy [eV]	Reference
$C_{10}H_7^+$	H	15.4	42, 45, 47, 51
$C_8H_6^+$	C_2H_2	15.4	42, 45, 47, 51
$C_6H_6^+$	C_4H_2	15.5	42, 45, 51
$C_{10}H_6^+$	H_2	15.9	42, 45
$C_7H_5^+$	C_3H_3	16.0	42, 51
$C_8H_5^+$	$C_2H_2 + H$	18.5	42, 45
$C_6H_4^+$	$2C_2H_2$	18.5	42, 45
$C_6H_5^+$	$C_2H_2 + C_2H$	18.6	42, 45, 51
$C_3H_3^+$	$C_3H_3 + C_4H_2$	19.3	42, 51
$C_4H_4^+$	$C_4H_2 + C_2H_2$	19.5	42, 45
$C_5H_3^+$	$C_2H_2 + C_3H_3$	19.7	51, 42
$C_7H_3^+$	$C_3H_3 + H_2$	20.7	51
$C_4H_2^+$	$3C_2H_2$	20.7	42
$C_6H_3^+$		20.8	45
$C_4H_3^+$	$2C_2H_2 + C_2H$	22.3	42

B. Biphenylene

Biphenylene ($C_{12}H_8$) is a molecule exhibiting features which are typical for both, aromatics and anti-aromatics. Considering only the outer perimeter, biphenylene corresponds to an anti-aromatic annulene,[58] however, due to the weak interaction between the two ring systems it can also be regarded as a coupled pair of benzene rings and should be aromatic. Neither description is fully appropriate, and the behavior of biphenylene is often considered as an intermediate between aromatic and anti-aromatic.[59]

The absorption spectrum of biphenylene has been studied in the vapor phase.[60,61] With an even number of electrons biphenylene possesses a singlet ground state, S_0. The origin of the lowest excited singlet state, S_1, in gaseous biphenylene lies at 25 320 cm^{-1} (3.14 eV). The second excited singlet state, S_2, in the gas phase lies at 28 170 cm^{-1} (3.49 eV). The first photon, of the photolysis pulse, at $\tilde{\nu}_0 = 32\,468$ cm^{-1} (308 nm) will excite the molecule in the S_2 vibronic manifold. The relaxation from the excited singlet states of biphenylene is dominated by fast internal conversion (IC) transitions.[62–64]

TABLE II. Summary of appearance energies of biphenylene fragments.

Cationic product	Neutral product	Average appearance energy [eV]	Reference
$C_{12}H_7^+$	H	14.48	44
$C_{12}H_6^+$	H_2	17.30	44
$C_{10}H_6^+$	C_2H_2	15.57	44
$C_{10}H_5^+$	C_2H_3	18.66	44
$C_6H_4^+$	C_6H_4	19.68	44
$C_6H_3^+$	C_6H_5	21.87	44

1. Fragmentation of biphenylene

The IP of biphenylene was measured in the gas phase to be (7.56 ± 0.05) eV.[65] Therefore, after absorption of a second photon, biphenylene will undergo photolysis. Photo-ion mass spectrometry was used to obtain the parent and fragment photo-ion yields in the 8–35 eV range, using monochromatized synchrotron radiation.[44,52] Biphenylene fragments were found to form at excitation energies ≥ 14.48 eV (Table II). H, C_2H_2, and H_2 are the first neutral products formed from fragmentation, at 14.48 eV, 15.57 eV (which is less than the 4-photon excitation energy), and 17.3 eV respectively. The vacuum ultraviolet peak energy of parent photo-ion yield spectra was measured to be 17.3 eV.[44]

Among the similarities between naphthalene and biphenylene, the resemblance of the fragmentation channels after photolysis is most relevant for the results presented here. The appearance energies of fragments formed from naphthalene and biphenylene are summarized in Tables I and II. H, H_2, and C_2H_2 fragments can form following high energy monochromatized synchrotron radiation of naphthalene and biphenylene.[42,44,51,52] The energies at which most fragments appear, differ for naphthalene and biphenylene, however, the energies at which C_2H_2 fragments are produced are comparable. C_2H_2 fragments appear at excitation thresholds of 15.40 and 15.57 eV for naphthalene and biphenylene, respectively. C_2H_2 fragments can be formed from naphthalene through eight different channels below 22 eV. However, only one channel has been established for biphenylene. The ion fragments $C_{10}H_6^+$, $C_6H_4^+$, and $C_6H_3^+$ have also been observed after photolysis of naphthalene and biphenylene in Refs. 42, 44, and 51. Even though the formation thresholds of the two smaller ion fragments differ, the minimum formation energies of $C_{10}H_6^+$ are similar (15.90 and 15.57 eV for naphthalene and biphenylene, respectively), and as low as that for C_2H_2 abstraction. The similarities of specific fragmentation energies are important for the discussion in Sec. VI B, where the growth of the hydrocarbon fragments into particles will be discussed.

III. EXPERIMENT

The experimental setup is shown schematically in Figure 3. The gas mixtures were kept in an unstirred static vacuum chamber ($V \sim 5.3$ dm^3), which was filled with a small amount of naphthalene vapor (scintillation grade, >99% Aldrich, CAS 91-20-3) buffered by a noble

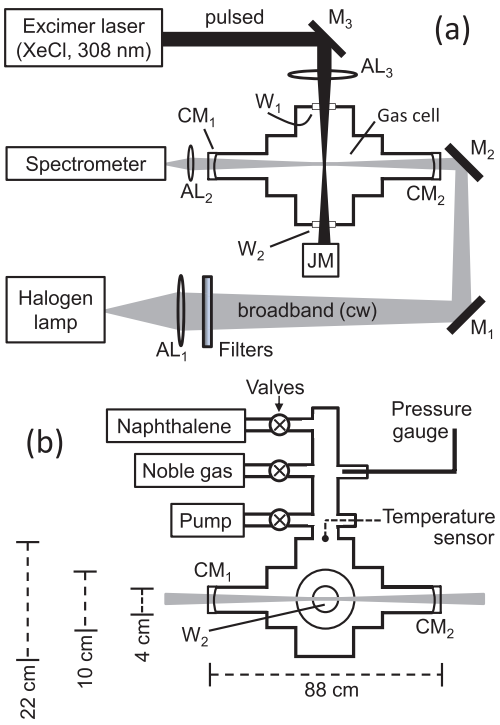

FIG. 3. (a) Experimental schematic (top elevation). AL_i: achromatic lens, M_i: aluminium mirrors, W_i: fused silica windows, CM_i: (high reflectivity) cavity mirrors, JM: Joule (energy) meter. (b) Side elevation: Schematic of the six-way cross center piece ($V \sim 3.8$ dm^3) of the static unstirred gas chamber ($V \sim 5.3$ dm^3).

gas. The partial pressure of naphthalene, P_{Nap}, was kept at the vapor pressure of naphthalene at room temperature (∼0.068 mbar)[66] in most experiments. The buffer gases used were helium (grade 5) and argon (grade 4.8) at typical pressures between $5 < P_{He} < 135$ mbar for He and $5 < P_{Ar} < 30$ mbar for Ar. The pressure and temperature inside the chamber were monitored by a membrane gauge (Leybold, Cervac CTR 90) and a platinum resistance thermometer (Lakeshore, PT-11), placed ∼10 cm above the center of the chamber. Naphthalene was excited at 308 nm using a pulsed excimer laser (Lumonics EX-700, XeCl). The UV light was focused with a quartz lens (focal length 30 cm) into the center of a six-way cross-piece (Figure 2) where photolysis of the PAH vapor took place. The laser pulse energies, E_{pulse}, were typically between 2 and 100 mJ measured with a Joule meter (Gentec, ED-500L). At a pulse duration of ≈15 ns (FWHM), these energies correspond to maximum photon fluences of ∼0.01–0.34 × 10^{12} W cm^{-2}, assuming a beam waist of roughly ∼50 μm in the focal plane of the lens. At these high fluences, resonance enhanced n-photon absorption ($n > 1$) can become very efficient, leading to ionization and fragmentation of naphthalene (see Sec. II A). It is important to note that the range of excitation irradiances is still significantly below the laser induced breakdown thresholds of helium and argon. The breakdown limits for argon and helium were measured in Ref. 67 as a function of the gas pressure using 18 ns pulses of an excimer laser (KrF) at 248 nm. The breakdown threshold of argon under these irradiation conditions increases monotonically from ≈0.05 × 10^{12} W cm^{-2} at

$\sim$1000 mbar to $\approx 20 \times 10^{12}$ W cm^{-2} at $\sim$10 mbar. For helium, the breakdown limits are even higher, i.e., $\approx 1 \times 10^{12}$ W cm^{-2} at $\sim$4000 mbar, and $\sim 20 \times 10^{12}$ W cm^{-2} at 240 mbar.[67] The reported lower limits of the breakdown irradiance in the low pressure regime are hence >60 times larger than those applied in our measurements at approximately the same gas pressures. Since a shorter excitation wavelength was used in Ref. 67, it is safe to assume that no laser induced breakdown of the buffer gas took place during the experiments. Furthermore, field ionization due to the local electric field generated by the focused laser pulse is not operative at our maximum power densities of 0.2×10^{12} W cm^{-2}, which corresponds to ≈ 1.23 V nm^{-1}.[43]

Extinction before and after UV photolysis was measured using IBBCEAS.[19] In IBBCEAS, an optically stable cavity formed by two highly reflecting mirrors (with geometric mean reflectivity R) is continuously excited with incoherent light. The intensity of light transmitted by the cavity is measured first without sample losses (I_0) and then with a sample in the cavity (I). For small losses per pass and high reflectivities of the mirrors, the extinction (absorption and scattering) of the sample (ε) is given by[19]

$$\varepsilon(\lambda) = \frac{1 - R(\lambda)}{d} \left(\frac{I_0(\lambda)}{I(\lambda)} - 1 \right), \quad (1)$$

where d is the length over which light inside the cavity interacts with the sample, i.e., with the UV photolysis product(s). It is important to note that this path length d is not necessarily equal to the separation of the cavity mirrors (88 cm); d is not known for the present experiments and can only be estimated. Since spatial and time-dependent variations of the photolysis products in the photolysis chamber are also unknown, the loss per pass $L = \varepsilon d$ was measured as the most appropriate quantity in this context.

The cavity was set up along an axis perpendicular to the UV photolysis beam (see Figure 3). Losses induced by the naphthalene/buffer gas mixture before and after UV excitation were measured in two different wavelength regions: region (a) 390–620 nm and region (b) 550–850 nm. Between 390 and 850 nm, the absorption of neutral naphthalene is far too weak to be observed. Two pairs of mirrors (Layertec, radius of curvature = 2 m) with reflectivities $R = (R_1 R_2)^{0.5} = 0.995 \pm 0.003$ and $R = 0.990 \pm 0.003$ were used to cover regions (a) and (b), respectively. An important experimental aspect of IBBCEAS is the calibration of the cavity mirror reflectivity as a function of wavelength. In the 390–620 nm region (a), an antireflection-coated optical flat of well defined loss was used for reflectivity calibration (see Refs. 68 and 69); in the 550–850 nm region (b), a double beam absorption spectrometer (Perkin-Elmer, Lambda 1050) was used to verify the mirror reflectivity.

The broadband light source for all measurements was a light guide coupled halogen lamp (Leica, KL1500 LCD). Light exiting the light guide was focused with an achromatic lens (focal length 20 cm) into the center of the cavity. Fluctuations in the lamp intensity were monitored using a photodiode (Thorlabs, DET210); not included in Figure 3. For the short wavelength range (390–620 nm), a colored glass filter (Thorlabs, BG40) was used in front of the cavity, and a short pass filter (Edmund Optics) behind the cavity. For the long wavelength range (550–850 nm), only a long pass filter (Schott, OG550) was used in front of the cavity. Light exiting the optical cavity was collected with an achromatic lens (focal length 7 cm) and coupled into an optical light guide (1 mm diameter, 2 m length, transmission $\sim$80%), which was connected to a spectrometer (Ocean Optics, USB4000). The wavelength range of the spectrometer was 200–850 nm, with a resolution of 1.65 nm (FWHM) as measured using a low pressure mercury lamp. The integration time for light transmitted by the cavity was typically between 10 and 500 ms (depending on the combination of filters and mirrors utilized). To minimize sweep-to-sweep fluctuations (especially at short integration times), the time-integrated transmission was additionally averaged over several data acquisition duty cycles.

In a standard experiment, the stainless steel vessel was evacuated (10^{-3} mbar) by a rotary pump (Edwards, E2M8) before an appropriate amount of naphthalene was sublimed into the chamber at room temperature, which was subsequently filled with an appropriate amount of buffer gas.[70] The sample mixture was given time to equilibrate, possible temperature variations were generally smaller than $\pm$0.5 K (when the chamber temperature was controlled it was $<\pm$0.1 K). The sample was then exposed to a predefined number of UV laser pulses (typically between 10 and 1000) at repetition rates between 2 and 25 Hz. The loss spectra after multi-photon ionization/fragmentation were then recorded as a function of time, exhibiting unexpected dynamics.

Please note: In Ref. 24 (see also Sec. I), the time-dependent optical loss caused by the UV photolysis products was measured by means of the pulsed CRD method[25] employing a tunable dye laser (Lumonics, HD300) that was pumped by the same excimer laser (see Figure 1 in Ref. 24). The loss was measured at one fixed wavelength (typically at 650 nm), until the system was considered to be in equilibrium again. Ring-down times in the non-absorbing gas mixture before photolysis were typically $\tau_{crd} \sim 14$ μs for a 66 cm cavity length. The range of the smallest to the largest detectable extinction was $\sim 1.0 \times 10^{-7}$ cm^{-1} to 1.8×10^{-5} cm^{-1}, respectively. For each data point, at least ten ring-down transients were averaged, yielding a minimum time resolution of 3 s for our experiments. Only data presented in Sec. VI C 3 were measured using the setup in Ref. 24, all other data were taken using IBBCEAS with a time resolution as low as 10 ms.

IV. RESULTS ON NAPHTHALENE

The time-dependent optical losses reported in Ref. 24 were sensitive to the partial pressure of the buffer gases used, but also to that of naphthalene. Different buffer gas pressure regimes were used to classify the type of dynamic loss that can be expected from a certain gas mixture (cf. Sec. I). It is important to note that it was essential to saturate the chamber walls with photolysis product(s) (or potentially also naphthalene, or both) for the observed dynamic loss behavior to occur.[71] Depending on the level of wall contamination, the boundaries of the partial pressure regimes which are used to characterize the time-dependent behaviors types I, II, and III are not really well-defined. For example, quasi-oscillatory losses (type II) of gas-mixtures at helium partial pressures

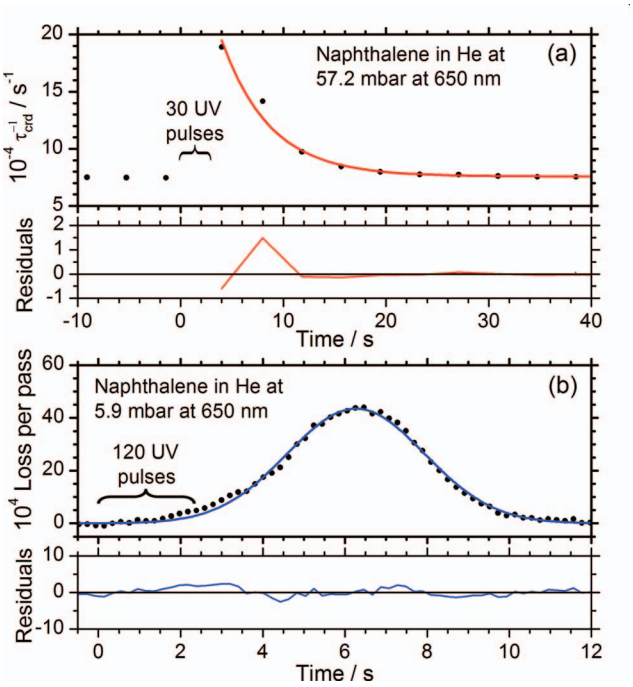

FIG. 4. (a) Sample mono-exponential decay behavior at 650 nm (dots) measured using the CRD setup; fit of mono-exponential function to data (red line) and the corresponding residuals. Fit parameters: decay time 4.7 s, max height 11.4×10^{-4} s^{-1}, offset 7.5×10^{-4} s^{-1}. Conditions: Excitation of naphthalene in 57.2 mbar of helium with 30 pulses at 20 Hz ($E_{\text{pulse}} \approx 25$ mJ). (b) Sample growth and decay behavior at 650 nm (dots) measured using the IBBCEAS setup; fit of Gaussian function to data (blue line) and the corresponding residuals. Fit parameters: center time 6.3 s, FWHM 3.9 s, loss amplitude 0.0043, loss offset 8.6×10^{-6}. Conditions: Excitation of naphthalene in 5.9 mbar of helium with 120 pulses at 50 Hz ($E_{\text{pulse}} \approx 24$ mJ).

below 75 mbar were not observed previously,[24] however, results obtained since then have produced quasi-oscillatory behavior below 75 mbar.

A. Type I: Growth and decay of optical loss (naphthalene)

At low buffer gas pressures (<75 mbar in helium), a "fast" rise in optical loss at 650 nm followed by a mono-exponential decay of the loss, with lifetimes between ~2 and ~23 s was reported in Ref. 24, using a CRD setup. This dynamical behavior was the most reproducible response of the system. The decay of the loss per pass at 650 nm was *empirically* described by a mono-exponential function (Figure 4(a)). The time $t = 0$ s was chosen as the time of the first UV pulse. The excitation time period is indicated in Figure 4. The data acquisition duty cycle of the CRD measurements was ~4 s.[24]

Due to the improvement in data acquisition speed by virtue of the IBBCEAS approach, with integration times as low as 10 ms, the time dependence of type I responses was revisited and enabled the monitoring of the growth of the optical loss as well as the decay at 650 nm (note: for the CRD experiment, only the decay could be monitored). It was found that the type I temporal behavior is best empirically described by a Gaussian function as exemplified in Figure 4(b). The Gaussian profiles fitted to the time dependent loss generally exhibited a somewhat larger rate of loss-increase than subsequent loss-decay, leading to a slight asymmetry in the temporal Gaussian profiles. This effect can be attributed to the fact that the duration of the UV excitation, which depends on the number of pulses and the repetition rate, is much larger than the time resolution of 10 ms in the IBBCEAS experiment. The better time resolution in comparison to the duty cycle of the CRD measurements (4 s) enabled the monitoring of the growth of loss, but also leads to an uncertainty in defining $t = 0$ s properly on the improved time scale. The Gaussian description of the time dependence worked, however, rather well in the vast majority of cases. Especially at lower buffer gas pressures (<10 mbar in helium), type I Gaussian profiles became increasingly symmetric with improved fit residuals. It was also established that in oscillatory type II responses the time dependence of the loss in many cases also followed a Gaussian behavior (an example is shown in Sec. SIII in the supplementary material[27]). At present there is no conclusive model that predicts the observed time dependence, the Gaussian description is purely *heuristic*.

B. Type II: Optical loss spectra with oscillatory time-dependence

1. Spectral region (a) 390–620 nm

A time-dependent loss measurement at 550 nm and loss per pass spectra *between* 390 *and* 620 nm, taken at four times (A…D) after laser photolysis are shown in Figures 5(a) and 5(b), respectively. The time-dependent loss per pass oscillates for ~70 min in the example shown in Figure 5(a). The initial extinction maximum (A) after excitation was followed by three maxima of increasing magnitude. After 20 min

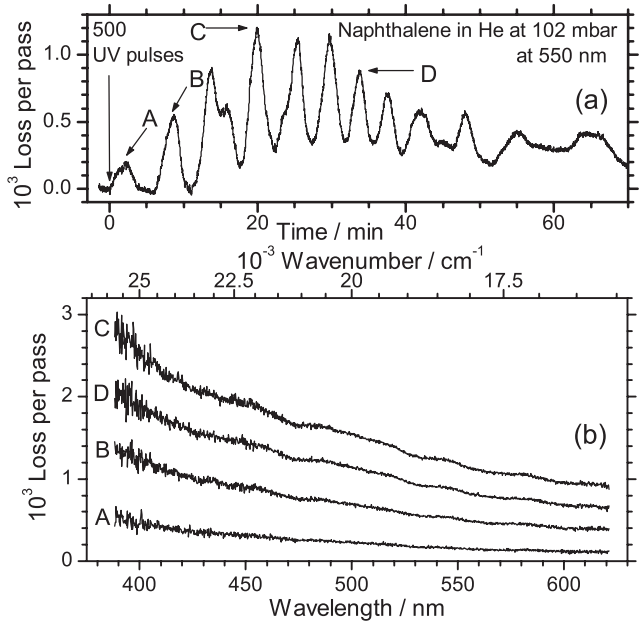

FIG. 5. (a) The first 75 min of time-dependent loss per pass at 550 nm. 500 pulses at 10 Hz with an average energy of 12.7 mJ began excitation of naphthalene, in 102 mbar of helium, at zero min. (b) Loss per pass spectra in the 390–620 nm region, A–D, as measured at times marked in panel (a). The lack of isolated features suggests that the source of loss is likely to be due to particles.

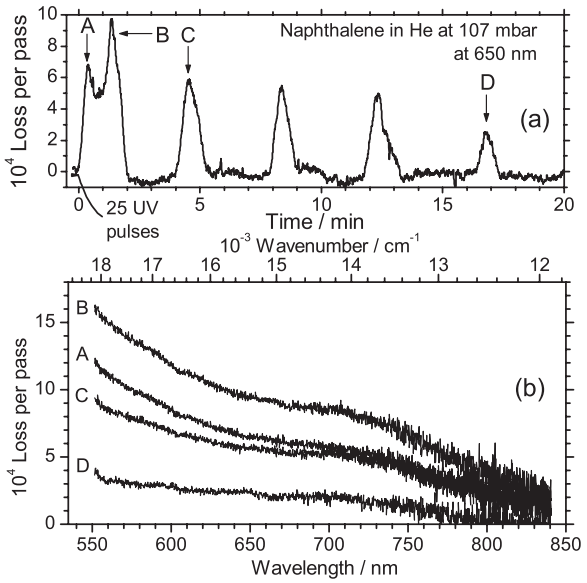

FIG. 6. (a) Time-dependent loss per pass at 650 nm. 25 pulses at 10 Hz with an average energy of 78.9 mJ began excitation of naphthalene, in 107 mbar of helium, at zero min. (b) Loss per pass spectra in the 550–850 nm region, A–D, as measured at times marked in panel (a). The lack of isolated features suggests that the source of loss is likely to be due to particles.

(fourth maximum), the magnitudes of the maximal extinction started to decrease.

As exemplified in Figure 5(b), the loss per pass spectra generally increase monotonically with decreasing wavelength. Small features appear at ∼471, ∼531, and ∼565 nm in some spectra (see C and D in Figure 5(b)). These features correlate with the calibrated wavelength-dependent reflectivity and are considered artefacts within the accuracy of the measurement. Spectra were measured using helium, neon, and argon buffer gases, at pressures of up to 400 mbar and at temperatures between 13.1 and 35.0 °C. Measurements were initiated using between 1 and 2000 UV pulses, with energies of up to ∼100 mJ and repetition rates up to 25 Hz (the typical conditions used are outlined in Sec. III). The absence of isolated features in all spectra suggests that the source of loss inside the chamber is unlikely to be due to absorption of molecular species but rather due to absorption and scattering by particles, concurring with measurements made in spectral region (b) (550–850 nm).

2. Spectral region (b) 550–850 nm

A time-dependent loss measurement at 650 nm and loss per pass spectra *between* 550 *and* 850 nm, taken at four times (A…D) after laser photolysis are shown in Figures 6(a) and 6(b), respectively. The time-dependent loss per pass oscillates for ∼17.6 min and consists of five extinction maxima; the first exhibiting two individual peaks. As exemplified in Figure 6(b), the loss per pass spectra generally increase monotonically with decreasing wavelength; a broad (weak) feature between ∼660 and ∼810 nm appears in virtually all spectra. Spectra were measured using helium, neon, and argon buffer gases, at pressures ranging from 5 to 120 mbar. Measurements were initiated using between 1 and 5000 UV pulses, with energies ranging from ∼2.5 to 92 mJ and repetition rates ranging from 5 to 25 Hz. Spectra recorded in the 550–850 nm range exhibit qualitatively the same wavelength dependence as those shown in Figure 5(b). The absence of isolated features again suggests that the source of loss inside the chamber is due to absorption and scattering by particles which must be formed after multi-photon photolysis. It proved impossible to overlap and concatenate the spectra in Figure 5(b) with the spectra in Figure 6(b) in a meaningful way. Due to the different responses of the gas mixture after UV photolysis, joining of spectra to cover 390–850 nm would not have been justified; arbitrary normalizations without quantitative knowledge of the source of the loss was deemed meaningless. A brief discussion of the potential photolysis products will be given in Sec. VI A; a more detailed analysis will be presented in a subsequent publication (unpublished).[28]

V. RESULTS ON BIPHENYLENE

In order to get an indication whether the observed behavior of naphthalene gas mixtures following photolysis is unique or indeed a more general phenomenon for different polycyclic hydrocarbons, experiments were performed using a different compound with appropriate vapor pressure, i.e., biphenylene ($C_{12}H_8$). As saturation of the chamber walls with photolysis products in the naphthalene experiments was crucial for dynamic behavior to occur, care was taken to thoroughly clean the chamber (including baking) before experiments with biphenylene commenced. In test measurements made to verify the cleanliness of the chamber, it was established that any effects that could potentially be due to vestiges of contaminants were negligible. Experiments performed using biphenylene were made over a period of less than three months, where initially the chamber had to be "passivated" with biphenylene.

Experiments on biphenylene were performed at four buffer gas pressures, ∼30, ∼50, ∼80, and ∼100 mbar. Comparable dynamic behavior, to naphthalene gas mixtures, was observed in biphenylene–helium mixtures following UV photolysis.

A. Type I: Growth and decay of optical loss (biphenylene)

Simple growth in optical loss followed by decay, type I behavior, was measured at helium buffer gas pressures of ∼30 mbar.

B. Type II: Optical loss spectra with oscillatory time-dependence

At the higher pressures, quasi-oscillatory behavior, type II, was observed. Figures 7(a1) and 7(a2) show two examples of type II dynamic behavior of loss per pass, at 550 and 650 nm, respectively.

The loss per pass spectra in the region (a) (400–620 nm) and region (b) (550–850 nm) are shown in Figures 7(b1) and 7(b2). The corresponding times of measurement are marked in panels (a1) and (a2) of Figure 7. In general, the loss per pass increased monotonically with decreasing wavelength. Weak features between 473 nm and 531 nm occurred in

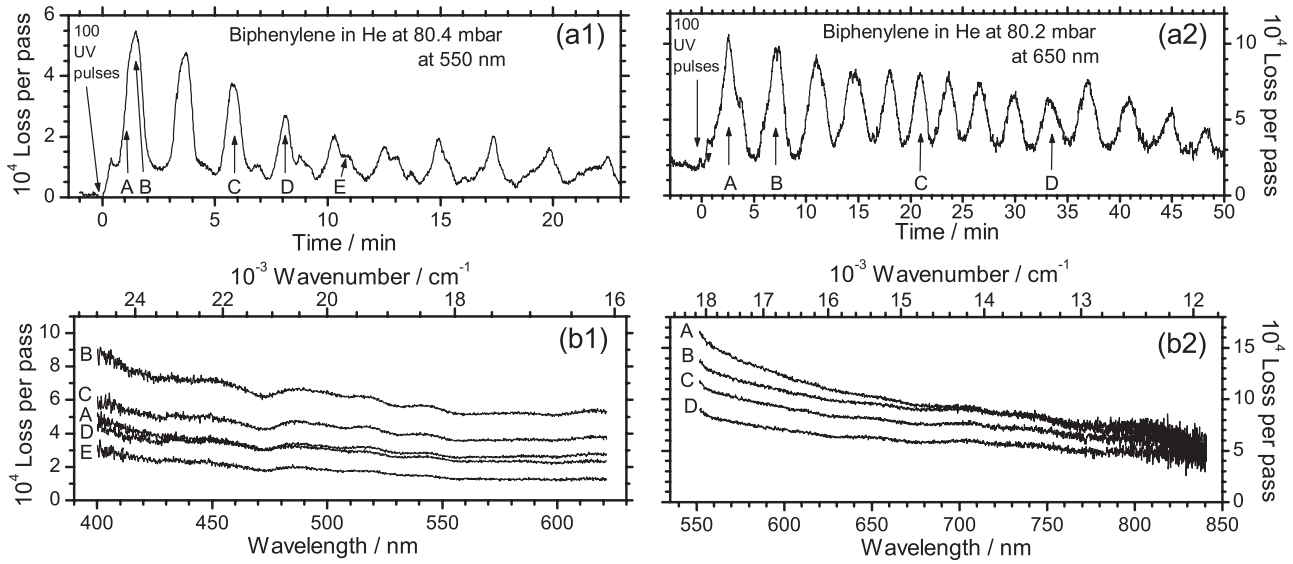

FIG. 7. Sample time-dependent loss per pass at 550 nm, panel (a1), and 650 nm, panel (a2), for biphenylene buffered with ~80 mbar of helium. 100 UV pulses at 5 Hz began excitation of biphenylene, at 0 min in both measurements. The average pulse energies for (a1) and (a2) were 18.2 and 96 mJ. Panels (b1) and (b2) show loss per pass spectra in regions (a) and (b), measured at times marked in panels (a1) and (a2). The lack of isolated features suggests that the source of loss is likely to be due to particles, similar to naphthalene mixtures following photolysis.

region (a), however, these features correlated with the measured root mean square reflectivity curve and were considered artefacts within the accuracy of the measurement. The broad feature between 775 nm and 840 nm occurred in some measurements in region (b). This latter feature was correlated with the root mean square reflectivity of the mirrors and was due to low lamp intensity in this wavelength range and thus does not represent genuine structure in the spectrum. The almost structureless extinction spectra of biphenylene after photolysis resemble those measured for naphthalene between 400 and 850 nm. The absence of isolated features suggests again that the observed loss is likely to be due to absorption and scattering by particles formed after photolysis. The study of biphenylene illustrates that the time-dependent behavior resulting from UV photolysis of naphthalene–buffer gas mixtures is not an isolated phenomenon among PAHs.

The buffer gas pressures of helium at which oscillations occur in biphenylene are similar to the pressures identified in Ref. 24 for naphthalene before the chamber became highly contaminated with species from previous experiments; i.e., no oscillations were found to occur at 30 mbar. This demonstrates the influence of the buffer gas pressure on the time-dependent behavior. Different PAHs at different pressures may result in oscillations; however, they will only occur depending on transport conditions in the chamber which depend on the buffer gas pressure. The ratio of the amount of contaminant on the wall to buffer gas pressure is also a factor that influences the dynamic extinction behavior, as the system becomes more complex with successive measurements.

VI. DISCUSSION

A. Considerations regarding molecular photoproducts

Molecular species that could potentially form in the UV excitation and cause or contribute to the spectra in Figs. 5 and 6 (Sec. VI) were considered,[26] but no obvious match or assignment could be made. A brief discussion is given here.

1. Naphthalene cation ($C_{10}H_8^+$)

$C_{10}H_8^+$ was formed with high probability[72] in the multiphoton excitation at 308 nm, but only as an intermediate considering the time scale of the experiments. Due to its ionic nature, it is not expected to be stable for the duration of many minutes in a stainless steel chamber. The absorption spectrum of the naphthalene cation was measured in an argon matrix[73] and in a supersonic jet,[74] however, none of the strongly allowed π–π transitions with strong absorption bands around 613 nm, 649 nm, and 671 nm were observed in the spectra. Hence, the naphthalene cation was discarded as the carrier of the oscillating extinction.

2. Azulene ($C_{10}H_8$)

Azulene is a stable isomer of naphthalene containing a five member and a seven member ring. In Ref. 75, a conversion from naphthalene to azulene by a 2 UV-photon (193 nm) absorption buffered in a 1000 mbar nitrogen atmosphere has been reported. In Ref. 49, the potential energy for the cationic naphthalene/azulene isomerization was estimated. The isomerization takes place below the energy required for the dissociation of the ion by C_2H_2 loss. Under the experimental conditions for which oscillations can be observed, it is conceivable that an isomerization may occur during the UV excitation phase of the experiment. However, a comparison of the spectra in Refs. 19 and 76 with the spectra here shows that azulene is not observable. Either the amount of azulene produced is too small to be detectable, or azulene is not formed due to photo-dissociation processes which may dominate for certain excitation energies.[77]

3. Other potential carriers

Absorption of four photons (≈16.1 eV) can cause the naphthalene molecule to fragment (Sec. II A 1). The benzene ion ($C_6H_6^+$) is one of the possible products appearing at the average energy of 15.7 eV.[51] The benzene ion is known[78] to have several strong absorption lines at ∼553 nm but none of them were observed in the spectrum. After recombination of the benzene ion, the electronic π–π^* transition ($S_1 \leftarrow S_0$) of benzene (C_6H_6) are in the UV region (∼266 nm). In the visible region, there are only very weak CH stretch overtones (4th, 5th, and 6th overtones at 711, 604, and 529 nm, respectively),[79] which were not observable in the extinction spectra in accordance with expectation.

Since the ionic fragments that may be formed in the UV excitation ($C_{10}H^{+7}$, C_8H^{+6}, C_6H^{+6}, $C_{10}H^{+6}$, C_7H^{+5}, C_8H^{+5}, C_6H^{+4}, C_6H^{+5}, C_3H^{+3}, C_4H^{+4}, C_5H^{+3}, C_7H^{+3}, C_4H^{+2}, C_6H^{+3}, and C_4H^{+3})[51] are very diverse, potentially a substantial number of stable species could form after the photolysis due to chemical reactions among them.

Even if none of the produced electrons recombines with an ion, the lifetime of the ions should be less than the diffusion time (∼10 s)[26] to the walls of the steel chamber. Thus, the amount of ions in the chamber is too small to be detected. An estimation of the number of naphthalene molecules in the photolysis region indicates that the oscillating absorption ($\alpha \sim 10^{-5}$ cm^{-1}) is not only due to primary photolysis products since the maximum concentration (2.3×10^6 molecules/cm^3) obtainable from photolysis is too low for such strong absorptions, assuming typical absorption cross-sections for allowed transitions of $\sigma \sim 10^{-17} \ldots 10^{-16}$ cm^2. This explains why neither azulene nor benzene absorption structures are observable in the measured spectra. The species produced upon UV multi-photon excitation must be either (i) a catalyst for the chemical production of absorbing species in a reaction scheme involving naphthalene (which is most abundant in the chamber), or (ii) particles which fulfill the condition of possessing sufficiently large cross-sections. We consider the latter possibility to be most likely and therefore discuss particle formation in the following Sec. VI B and outline additional observations supporting this hypothesis in Sec. VI C.

B. Considerations regarding particle formation

Chemical pathways to particle formation from PAHs has been studied greatly in the context of soot formation in combustion processes.[4,80,81] In such cases, the motivation to understand the chemical pathways leading to the formation of soot is mainly to avoid its generation, as soot generally represents an unwanted accumulating contaminant and potential health hazard. The majority of studies on soot formation concern shock-tube pyrolysis and laminar flame techniques.[5,6] There is considerable evidence that PAHs play a key role in soot formation, although other reaction pathways involving polyacetylenes and ionic species have been suggested.[82] There are several comprehensive reviews on the chemical pathways of soot formation;[4,80,81] generally four phases (P) in soot formation can be distinguished

P1: The phase in which small molecular precursors to soot (such as small aromatic species like benzene or naphthalene) are either present or formed.

P2: The growth phase of (aromatic) species, up to 500–1000 amu, by H-abstraction-C_2H_2-addition (HACA).

P3: The transition phase from gaseous species to solid particles (2000 amu) of diameters up to ∼< 1.5 nm.

P4: The phase of surface aging and particle coagulation.

In the current experiments, naphthalene or biphenylene molecules around the photolysis zone are abundant and the most likely (small) aromatic precursor to soot formation.[83] The growth phase of the initial aromatic species (here naphthalene or biphenylene) can be qualitatively described by HACA, which involves the repetitive reaction sequence of two principle steps:

Step 1. The abstraction of atomic hydrogen from the reacting hydrocarbon by a gaseous hydrogen atom,

$$A_i + H \rightarrow A_{i-} + H_2, \quad (2)$$

where A_i represents an aromatic molecule with i peri-condensed rings, and A_{i-} is its radical.

Step 2. Addition of gaseous acetylene to the radical formed,

$$A_{i-} + C_2H_2 \rightarrow \text{products}. \quad (3)$$

For *naphthalene*, the first two neutral species formed from the photolysis are H and C_2H_2 at 15.4 eV and there are a total of eight known channels for the formation of H and C_2H_2. The abundance of these neutral species in the chamber increases with each photolysis pulse. Hence, with increasing number of pulses the probability of soot formation increases and the increase in optical losses inside the cavity becomes detectable.

For *biphenylene*, the first two neutral species formed from the photolysis are also H and C_2H_2 at 14.48 eV and 15.57 eV, respectively.[44] Even though no definite reaction pathway is known for biphenylene, HACA is considered to be a generally applicable growth process of PAHs to soot. The key feature of the HACA steps is the reversibility of the reactions. The rate of the back-reaction of steps 1 and 2 are what hampers or accelerates molecular growth. The transition of heavy PAHs to nascent soot particles is the most poorly understood phase in soot formation. Increasing molecule growth can merely describe the mass of soot formed, and generally the final particle sizes are underestimated. The difficulty is that the nucleation processes is not purely chemical. PAHs form dimers during collisions based on di- or multi-polar interactions. PAH dimers collide with molecules or with other dimers to form larger complexes. The molecular complexes continue to grow based on physical interaction and chemical reactions to a critical size when PAH clusters evolve into solid particles. At some stage, the surface growth rate of the particles declines with the extent of particle growth, known as "soot surface aging." Once soot particles are formed collisions further increase particle sizes and decrease particle number densities without affecting the total mass of the soot. The particle coagulation involves coalescent growth and

particle agglomeration, which depend on the particle sizes and mean-free-path of the particles. In coalescent growth, the particles are generally assumed to be spherical; they coalesce completely, forming new spherical particles, which influences the dynamic spectral development of the loss per pass after photolysis. At some stage, the soot particles agglomerate. This process occurs after particle inception takes place.[84] As loss spectra show that the size distribution and refractive index of particles evolve on a timeframe of minutes, the last stages of soot formation clearly occur during oscillations and not immediately after photolysis, adding extra complexity to the description of the system. This aspect is further discussed in Sec. VI D (Fig. 9). A quantitative estimate of particle distributions and the modelling of the corresponding extinction spectra will be subject of a subsequent publication.[28]

C. Additional observations

1. Temperature dependency

Experiments were performed at 3 different gas mixture temperatures, ∼13.5 °C, ∼21 °C, and ∼34 °C, to study the influence of the temperature on the dynamic behavior of optical losses (see also Fig. S6 in the supplementary material[27]). Only in the experiments performed at ∼34 °C the ambient temperature outside the chamber was actively controlled by using a temperature controller inside a thermally controlled box built around the entire chamber. To achieve a temperature of ∼13.5 °C, a tube carrying thermalized water was wrapped all around the outside surface of the chamber. Experiments at ∼21 °C were performed at room temperature. The temperature fluctuation was ≈0.1 °C for all experiments. At each temperature, three experiments were performed at three different helium buffer gas pressures, i.e., 50 mbar, 80 mbar, and 100 mbar. In each experiment, 35 pulses, with approximately the same energy (17 mJ per pulse), were used to photolyze naphthalene at a repetition rate of 10 Hz. Oscillatory time-dependent behavior in the optical losses were observed in all measurements. At all three pressures, the smallest change in optical losses was found at ∼13.5 °C. Also at ∼13.5 °C the system appeared to return to equilibrium (i.e., to the "baseline" loss before excitation) the fastest, exhibiting the least complex behavior of all three temperatures. We were unable to establish whether temperature gradients persisted in the chamber that could give rise to convection currents (see also Sec. VI D 2).

2. Volume dependency

Since the walls of the chamber appeared to be an efficient sink for the photolysis products, their effect on the dynamic behavior of the system was further investigated by changing the wall surface-to-volume ratio. The six-way central cross-piece, $V \sim 3.8$ dm^3, of the chamber with an overall volume of 5.2 dm^3 was replaced with a significantly smaller four-way cross-piece, ∼0.46 dm^3. The total volume of the smaller chamber was 1.1 dm^3. The distance from the nearest wall surface to the photolysis region in the six-way crosspiece and four-way crosspiece were 5 cm and 2 cm, respectively. Measurements were performed in the 1.1 dm^3 chamber with helium buffer gas pressures ranging from 13 mbar to 500 mbar, using repetition rates ranging from 5 Hz to 20 Hz and pulse energies of up to 105 mJ. All measurements showed simple growth and decay behavior (type I). The fact that no oscillatory behavior was observed in the 1.1 dm^3 chamber suggests that the walls of the chamber inhibit the creation of oscillations due to adsorption of species created during photolysis to the chamber walls.

3. Stirring the gas mixture

The effect of stirring was investigated for types I and II behavior. A small 12 V fan (∼60 revolutions/s) was installed on the floor of the vacuum chamber ∼13 cm below the optical axis of the cavity. The dynamic behavior was studied for two situations:

(i) The stirring commenced before the photolysis of the gas mixtures:
   a. Type I: At low buffer gas pressures, the maximum optical loss in this situation was found to be lower than for the static mixture in all cases. The stirred mixture showed a slight increase in optical loss in the final state of the system after photolysis. Increased losses close to equilibrium were observed in most experiments.
   b. Type II: At higher buffer gas pressures, the system returned to equilibrium in less than 10 min in all cases, indicating the strong damping imposed on the system by the fan action. In all cases, the observed extinction was smaller than without stirring and in some cases only type I behavior was observed.

(ii) The stirring commenced after the photolysis of the gas mixtures:
   a. Type I: At low buffer gas pressures when stirring was commenced close to equilibrium, an increase in optical loss was observed occasionally. The interpretation of this observation is the likely detachment of particles from the chamber wall by the fan action, creating the increase in loss after the growth-and-decay behavior.[85]
   b. Type II: At higher buffer gas pressures when stirring was commenced while the optical loss of the system was oscillating, the oscillatory behavior stopped almost immediately. When the stirring was subsequently stopped, the oscillations did not reappear (an example is shown in Figure 8).

D. Considerations regarding the system's dynamics

All types of temporal responses were observed in all buffer gases suggesting that the buffer gas is not chemically important to the system, and does not undergo any reactions with naphthalene/biphenylene or the photolysis products. However, the dynamics of responses observed is largely dependent on the type and pressure of the buffer gas. Therefore, the temporal responses must depend strongly on the physical parameters and the transport properties of the buffer

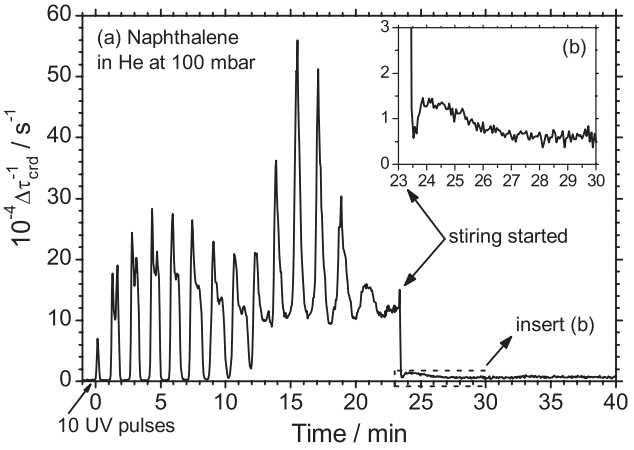

FIG. 8. (a) Sample time-dependent behavior of optical losses at 650 nm measured using the CRD setup and the effect of stirring the gas mixture, at ∼23 min, on the behavior. The optical loss falls immediately after stirring begins, but it then increases slightly before returning back to the baseline optical loss level. No further change in optical loss occurs following the initial slight increase. Conditions: Excitation of naphthalene in 100.5 mbar of helium with 10 pulses at 10 Hz ($E_{pulse} \approx 24$ mJ). (b) The inset shows an enlargement of the dashed time regime when stirring commenced.

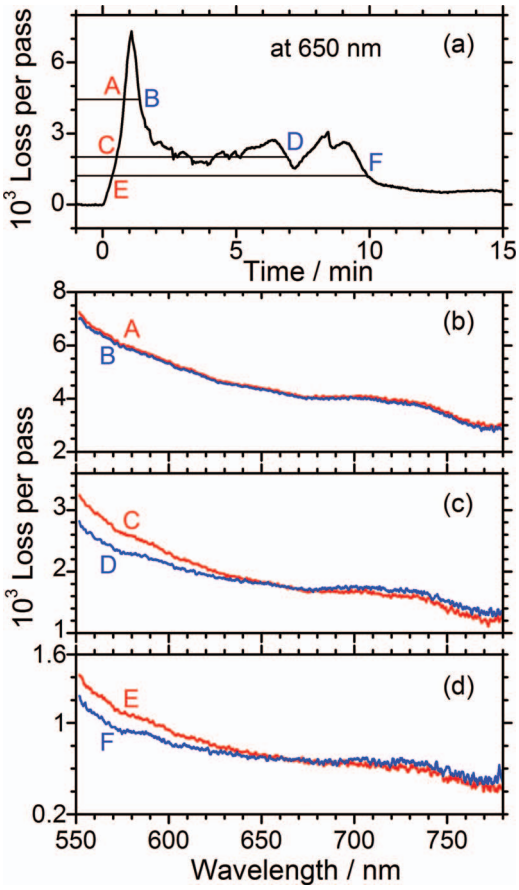

FIG. 9. (a) Time-dependent loss per pass at 650 nm after excitation of naphthalene in 96 mbar of helium with 2000 UV pulses at 10 Hz with an average energy of 8.2 mJ. The broadband spectra recorded at the times marked A…F are shown in the three lower panels. (b) Loss per pass spectra at times A and B. (c) Loss per pass spectra at times C and D. (d) Loss per pass spectra at times E and F. Each pair of spectra A and B, C and D, E and F have the same loss per pass at 650 nm as indicated by horizontal lines in panel (a).

gas. Stirring the system has the effect of disrupting any transport occurring in the system, indicating again that transport processes in the system play a crucial role in its temporal development.

1. Type I

The time dependence of type I responses can be conceptually explained by the initial formation of photoproducts inside the probing light path and their subsequent diffusion out of the optical cavity, provided that the walls act as an effective sink for the photoproducts and inhibit their return into the probing light path. Two regions are of relevance, (a) the photolysis volume, and (b) the volume of the probing light, which are both assumed to be cylindrical. The typical diffusion time for a molecule to diffuse from the axis of a cylinder, of radius A, to the edge of the cylinder is given by[86]

$$t_D = \frac{A^2}{5.8D}, \tag{4}$$

where the diffusion coefficient $D = 1.6$ cm^2 s^{-1} was calculated from the vapor pressure of naphthalene at room temperature in 10 mbar helium – see Sec. SV in the supplementary material.[27] Assuming a radius of the cylindrical photolysis volume of $A = 50$ μm yields a diffusion time of ≈2.7 μs, while for the probing light volume with $A = 9$ mm a diffusion time of ≈87 ms can be estimated (Note: the time scale for diffusion from the center of the chamber to the walls at a distance of ∼10 cm is ≈10.8 s). Thus, for a typical laser repetition rate of, e.g., 10 Hz, the photolysis zone was replenished with new sample of naphthalene between UV pulses and new photoproducts were formed with each pulse. The time scales established here are in agreement with the observed responses of type I (cf. Fig. 4), especially if immediately after each laser pulse the photoproducts form particles, whose diffusion time can be significantly longer depending on the particle size. To determine the diffusion time of particles, their size distribution and concentration must be known. Description of the typical size distribution of particles formed after photolysis will be the focus of future work.[28]

2. Type II (and III)

At conditions of higher buffer gas pressures where photoproducts/particles are kept away from the walls of the chamber for much longer, type II (and III) responses were observed. The time dependent nature of the optical loss indicates that convection currents[87] or other forms of turbulence or fluctuations are dominating the type II behavior. When particles are "carried around the chamber in convection currents," a loss maximum is observed when the convection causes the particles to move into or across the probing light volume in the cavity. Different convection currents with different initial and boundary conditions would then yield different responses. It is not clear whether general temperature instabilities could drive the convection currents. The initial temperature gradient generated by the excitation process appears insufficient in this context as the following upper-limit-estimate illustrates:

If each naphthalene molecule in the photolysis region (cylindrical volume of radius 50 μm and length 1 mm, $n\sim6 \times 10^{10}$ cm^{-3}), $\sim1.2 \times 10^{10}$ molecules, absorbed 5 photons, the total energy deposited in the focus per pulse would be 3.8×10^{-8} J. In helium at 10 mbar, the number of helium atoms in the photolysis region is $\sim2 \times 10^{12}$. With a heat capacity of helium of $\sim$5170 J kg^{-1} K^{-1},[88] the photolysis energy would result in a local temperature increase of <600 K. However, this corresponds to a maximum temperature rise in the entire gas of the order of $\sim10^{-6}$ K per UV pulse, assuming no heat transfer to the walls. As the chamber is not thermally isolated ($T = \pm0.1$ K), it appears impossible that convection currents could still be driven by the initial temperature change after many tens of minutes for a typical type II response. A reasonable explanation for the rather striking oscillations of the optical loss cannot be given at present and no experimental results, which can be directly compared with the data obtained, could be found in the literature.

However, oscillating absorption of light due to transport has been reported in the liquid phase. Damped oscillations, with periods of 30–60 s, of the absorption of 1,5-diaryl-3-alkyl-pentazadiene monomers and polymers, in a temperature controlled cuvette, induced by pulsed UV irradiation (at 308 nm) has been reported.[89] Absorption inhomogeneities produced by the laser irradiation combined with a convection current induced by the temperature stabilizing system resulted in the oscillations.[90] The period of oscillations could be determined through the stabilization temperature and the boundary conditions for the liquid phase study were generally better defined. Despite similarities concerning the necessity for convection currents between the work in Ref. 89 and the dynamic behavior described here, the types of oscillations in this work are more diverse, with often multiple components oscillating, allowing only a qualitative description of the phenomenon. The chamber walls in the present case act as inhibitor for oscillations and the efficiency of damping cannot easily be defined, whereas in the cuvette, the damping of oscillations was due to diffusive mixing.

More diverse oscillating behavior has been observed in the fluorescence intensity of dilute solutions of anthracene and 9,10-dimethylanthracene in chloroform illuminated with light from a Xe-Arc lamp at constant intensity.[91] The dynamic behavior of the emitted light included quasi-periodic oscillations, with sometimes multiple peaks, and more complex behavior. The constant illumination of liquid samples, kept the system far from equilibrium throughout the dynamic behavior. The reproducibility of the systems response was also found to be difficult. In all cases, the observed oscillations resulted from convection motion of the liquid in the cell.[92] Stirring the liquid or uniform illumination of the cell also destroyed the oscillations by eliminating inhomogeneities. The frequently observed aperiodicity and lack of reproducibility resulted from the extreme sensitivity of the convective motion to mechanical and thermal perturbations, resulting in no complete model of the systems being made.[92] Similar features were obtained with the gas-phase setup presented here, suggesting that the probable source of non-reproducibility was the sensitivity to convective currents in the system. A key difference between our experiments and the work in Ref. 91 is the initial input of energy in the form of laser pulses as opposed to continuous illumination. The gas-phase system remained away from equilibrium for up to hours. Moreover, the damping of oscillations, by the chamber walls, was an added uncertainty in the experiments presented here.

Finally, transport alone may not be sufficient to describe the observed features of the PAH/buffer gas mixtures. Although in the liquid phase complex oscillations can be described solely by convection currents, in those cases no physical or chemical change occurred to the absorbing species during oscillations. In contrast in the current setup, the evolving size distribution and refractive indices of the particles need to be taken into account to explain the observed absorption.

3. Time-dependence of the spectra

Due to the lack of isolated features in the loss per pass spectra in Figures 5 and 6, the size distribution of particles causing the loss and its dynamics, is not immediately obvious. To determine a time-dependence of the particle size distribution, if any, loss spectra recorded at different times during the experiment but with the same loss at a particular wavelength were compared. Figure 9(a) shows the first 15 min of a type III time-dependent loss per pass measurement at 650 nm. The measurement was made using 96 mbar of helium buffer gas, 2000 UV pulses at 10 Hz with an average energy of 8.2 mJ. Loss per pass spectra between 550 and 780 nm, taken at different times with equal loss per pass at 650 nm, are shown in Figures 9(b)–9(d). From the different loss per pass spectra shown in Figure 9, it is clear that the size distribution of particles causing the observed losses and possibly their refractive index are time-dependent and change over time. This behavior was observed in almost all measurements. Hence, a simple transport model of particles is insufficient to describe the observed behavior and the changing particle properties (due to agglomeration) must also be taken into account.

A complete model of the dynamic behavior is still out of reach. For such a model, a number of parameters need to be determined;

(1) The size distribution of particles and refractive index of the particles in the chamber.
(2) The evolution of the size distribution and refractive index of particles with time.
(3) The efficiency of the wall as a sink at different buffer gas pressures must be understood.
(4) The complex convection currents created in the gas mixtures following photolysis and how they evolve.

VII. CONCLUSIONS

The continued investigation of an oscillatory gas phase system (based on static naphthalene gas photolysis products), initially reported in Ref. 24, has revealed the complexity of the system's dynamic and new fascinating properties. The time-dependent broadband extinction of naphthalene–buffer gas mixtures following UV photolysis was measured between 390 nm and 850 nm, using IBBCEAS. The types (I, II, and II) of time-dependent extinction behavior reported in Ref. 24

were confirmed and refined. In all spectra involving naphthalene gas mixtures, the optical losses increased with decreasing wavelength and only a single broad feature was observed, between 660 nm and 810 nm. The lack of isolated features indicates that the observed optical losses are due to the absorption and scattering of light by particles. Other arguments in support of this interpretation have been presented in the paper based on the variation of parameters that govern the physical properties of the system; i.e., the temperature of the gas mixture and chamber walls, the chamber volume, stirring of the gas mixture, and the buffer gas pressure. The time-dependent behavior was found to depend profoundly on all parameters. More information on the dynamics of the extinction and potentially also on the nature of the particles could be obtained in future experiments by the insertion of carbon grids used for transmission electron microscopy at strategic points in the chamber.[93] Measurements made using biphenylene, as a substitute for naphthalene, showed that the unusual extinction behavior is a phenomenon that is not limited to naphthalene, but more general in nature as far as polycyclic hydrocarbons are concerned.

The discovery that particles are the dominant source of the optical losses shows that the oscillatory dynamics of the extinction is not based on the nonlinear chemical kinetics of a pure gas phase system. The active fragmentation channels during the photolysis and the subsequent chemical and physical particle formation mechanism (whose details are unknown as of yet) are crucial for initiating the time-dependent oscillatory behavior. In contrast to soot formation in flames, which occurs on a timescale of milliseconds, the photoproducts gradually grow/agglomerate into particles for a number of seconds after pulsed UV photolysis, and the system evolves on timescales of minutes up to hours. The long dynamics of the system is based on transport features of the system as well as particle interactions.[28] The competing processes in the oscillations are convection currents, coagulation, sintering, and deposition on the chamber wall.

The unusual discoveries outlined here in conjunction with well-studied PAHs, such as naphthalene and biphenylene, may have an impact on research into (i) combustion chemistry and soot formation, (ii) aerosol formation in atmospheric chemistry, e.g., in the context of simulation chamber studies, (iii) carbon grain growth in the interstellar medium and general astro-chemistry.

ACKNOWLEDGMENTS

The authors would like to thank Mr. J. Sheehan, Mr. J. Lucey, and Mr. C. Roche from the mechanical workshop of the Physics Department at UCC for their excellent technical assistance. We would like to thank Dr. S. Fiedler for useful discussions on the subject. This work was supported by the Basic Research Grant Scheme from Enterprise Ireland (contract: SC/2003/96) and by the Higher Education Authority (HEA–PRTLI3 scheme). A.A.R. acknowledges the support through the Science Foundation Ireland (SFI) Research Frontier Programme (contract: 11/RFP/3233). The authors are grateful for the very constructive suggestions by the reviewers to improve this article and the way the data are presented. Indeed reviewer 1 presented us with very clever ideas as to how to continue this experimental endeavour.

[1] D. A. Kaden, R. A. Hites, and W. G. Thilly, Cancer Res. **39**, 4152–4159 (1979).
[2] J. L. Durant, W. F. Busby, A. L. Lafleur, B. W. Penman, and C. L. Crespi, Mutat. Res./Genet. Toxicol. **371**, 123–157 (1996).
[3] D. C. Siegla and G. W. Smith, *Particulate Carbon Formation During Combustion* (Plenum Press, New York, 1981).
[4] H. Richter and J. B. Howard, Prog. Energy Combust. Sci. **26**, 565–608 (2000).
[5] J. Z. Wen, M. J. Thomson, M. F. Lightstone, and S. N. Rogak, Energy Fuels **20**, 547–559 (2006).
[6] I. Naydenova, M. Nullmeier, J. Warnatz, and P. A. Vlasov, Combust. Sci. Technol. **176**, 1667–1703 (2004).
[7] C. Moreau, E. Therssen, X. Mercier, J. F. Pauwels, and P. Desgroux, Appl. Phys. B **78**, 485–492 (2004).
[8] Y. Bouvier, C. Mihesan, M. Ziskind, E. Therssen, C. Focsa, J. F. Pauwels, and P. Desgroux, Proc. Combust. Inst. **31**, 841–849 (2007).
[9] M. Obst, P. Grathwohl, A. Kappler, O. Eibl, N. Peranio, and T. Gocht, Environ. Sci. Technol. **45**, 7314–7322 (2011).
[10] A. Eiguren-Fernandeza, A. H. Miguela, J. R. Froinesa, S. Thurairatnama, and E. L. Avolb, Aerosol Sci. Technol. **38**, 447–455 (2004).
[11] P. Pistikopoulos, H. M. Wortham, L. Gomes, S. Masclet-Beyne, E. Bon-Nguyen, P. A. Masclet, and G. Mouvier, Atmos. Environ., Part A **24**, 2573–2584 (1990).
[12] H. O. Pye and G. A. Pouliot, Environ. Sci. Technol. **46**, 6041–6047 (2012).
[13] A. G. G. M. Tielens, Annu. Rev. Astron. Astrophys. **46**, 289–337 (2008).
[14] F. Salama and L. J. Allamandola, J. Chem. Soc., Faraday Trans. **89**, 2277–2284 (1993).
[15] *The Diffuse Interstellar Bands*, Astrophysics and Space Science Library Vol. 202, edited by A. G. G. M. Tielens and T. P. Snow (Kluwer Academic Publishers, Dordrecht, 1995).
[16] F. Salama, G. A. Galazutdinov, J. Krelowski, L. Biennier, Y. Beletsky, and I.-O. Song, Astrophys. J. **728**, 154 (2011).
[17] L. J. Allamandola, A. G. G. M. Tielens, and J. R. Barker, Astrophys. J. **290**, L25–L28 (1985).
[18] A. Leger and J. L. Puget, Astron. Astrophys. **137**, L5–L8 (1984).
[19] S. E. Fiedler, A. Hese, and A. A. Ruth, Chem. Phys. Lett. **371**, 284–294 (2003).
[20] S. E. Fiedler, G. Hoheisel, A. A. Ruth, and A. Hese, Chem. Phys. Lett. **382**, 447–453 (2003).
[21] I. R. Epstein and J. A. Pojman, *An Introduction to Nonlinear Chemical Dynamics: Oscillations, Waves, Patterns, and Chaos* (Oxford University Press, New York, 1998).
[22] P. M. Gray and S. K. Scott, *Chemical Oscillations and Instabilities: Nonlinear Chemical Kinetics* (Clarendon Press, Oxford, 1990).
[23] *Oscillations and Traveling Waves in Chemical Systems*, edited by R. J. Field and M. Burger (Wiley-Interscience, New York, 1985).
[24] A. A. Ruth, E. W. Gash, M. Staak, and S. E. Fiedler, Phys. Chem. Chem. Phys. **4**, 5217–5220 (2002).
[25] *Cavity Ring-down Spectroscopy: Techniques and Applications*, edited by G. Berden and R. Engeln (Wiley-Blackwell, Chichester, 2009).
[26] E. Gash, Ph.D. thesis, University College Cork, Cork, 2004.
[27] See supplementary material at http://dx.doi.org/10.1063/1.4816003 for Secs. SI–SV.
[28] A. J. Walsh and A. A. Ruth, "Time-dependent size parameters and optical properties of particles formed following multi-photon UV photolysis of gaseous naphthalene," J. Chem. Phys. (unpublished).
[29] M. A. Duncan, T. G. Dietz, and R. E. Smalley, J. Chem. Phys. **75**, 2118–2125 (1981).
[30] D. E. Cooper, R. P. Frueholz, C. M. Klimcak, and J. E. Wessel, J. Phys. Chem. **86**, 4892–4897 (1982).
[31] A. Hiraya, Y. Achiba, N. Mikami, and K. Kimura, J. Chem. Phys. **82**, 1810–1817 (1985).
[32] M. C. R. Cockett, H. Ozeki, K. Okuyama, and K. Kimura, J. Chem. Phys. **98**, 7763–7772 (1993).
[33] M. Stockburger, H. Gattermann, and W. Klusmann, J. Chem. Phys. **63**, 4519–4528 (1975).
[34] U. Boesl, H. J. Neusser, and E. W. Schlag, Chem. Phys. Lett. **31**, 1–6 (1975).
[35] H. Gattermann and M. Stockburger, J. Chem. Phys. **63**, 4541–4545 (1975).

[36]M. Hassouna, J. L. Le Garrec, C. Rebrion-Rowe, D. Travers, and B. R. Rowe, "Reactions of electrons with hydrocarbon cations: From linear alkanes to aromatic species," in *Dissociative Recombination of Molecular Ions with Electrons*, edited by S. L. Guberman (Kluwer Academic, New York, 2003), pp. 49–57.
[37]D. Romanini, L. Binnier, F. Salama, A. Kachanov, L. J. Allamandola, and F. Stoeckel, Chem. Phys. Lett. **303**, 165–170 (1999).
[38]T. Pino, N. Boudin, and P. Bréchignac, J. Chem. Phys. **111**, 7337–7347 (1999).
[39]P. Bréchignac, T. Pino, and N. Boudin, Spectrochim. Acta, Part A **57**, 745–756 (2001).
[40]J. Krelowski, Adv. Space Res. **30**, 1395–1407 (2002).
[41]P. J. Sarre, J. Mol. Spectrosc. **238**, 1–10 (2006).
[42]H. W. Jochims, H. Rasekh, E. Rühl, H. Baumgärtel, and S. Leach, Chem. Phys. **168**, 159–184 (1992).
[43]M. J. DeWitt and R. J. Levis, J. Chem. Phys. **102**, 8670–8673 (1995).
[44]H. W. Jochims, E. Rühl, H. Baumgärtel, S. Tobita, and S. Leach, Int. J. Mass Spectrom. **167–168**, 35–53 (1997).
[45]R. J. van Brunt and M. E. Wacks, J. Chem. Phys. **41**, 3195–3199 (1964).
[46]X. Wang, H. Becker, A. C. Hopkinson, R. E. March, L. T. Scott, and D. K. Böhme, Int. J. Mass Spectrom. **161**, 69–76 (1997).
[47]Y. Gotkis, M. Oleinikova, M. Naor, and C. Lifshitz, J. Phys. Chem. **97**, 12282–12290 (1993).
[48]S. P. Ekern, A. G. Marshall, J. Szczepanski, and M. Vala, J. Phys. Chem. A **102**, 3498–3504 (1998).
[49]W. Cui, B. Hadas, B. Cao, and C. Lifshitz, J. Chem. Phys. **104**, 6339–6344 (2000).
[50]J. A. Syage and J. E. Wessel, J. Chem. Phys. **87**, 3313–3320 (1987).
[51]H. W. Jochims, E. Rühl, H. Baumgärtel, S. Tobita, and S. Leach, Astrophys. J. **420**, 307–317 (1994).
[52]H. W. Jochims, H. Baumgärtel, and S. Leach, Astrophys. J. **512**, 500–510 (1999).
[53]G. Granucci, Y. Ellinger, and P. Boissel, Chem. Phys. **191**, 165–175 (1995).
[54]Y. Ling and C. Lifshitz, Chem. Phys. Lett. **257**, 587–591 (1996).
[55]K. Schroeter, D. Schröder, and H. Schwarz, J. Phys. Chem. A **103**, 4174–4181 (1999).
[56]A. J. Midey, S. Williams, S. T. Arnold, I. Dotan, R. A. Morris, and A. A. Viggiano, Int. J. Mass Spectrom. **195–196**, 327–339 (2000).
[57]H. Abouelaziz, J. C. Gomet, D. Pasquerault, B. R. Rowe, and J. B. A. Mitchell, J. Chem. Phys. **99**, 237–243 (1993).
[58]N. Ohta, M. Fujita, H. Baba, and H. Shizuka, Chem. Phys. **47**, 389–394 (1980).
[59]Z. B. Maksic, D. Kovacek, M. Eckert-Maksic, M. Bockmann, and M. Klessinger, J. Phys. Chem. **99**, 6410–6416 (1995).
[60]R. M. Hochstrasser, Can. J. Chem. **39**, 765–772 (1961).
[61]I. Zanon, J. Chem. Soc., Faraday Trans. 2 **69**, 1164–1171 (1973).
[62]J. Hertzberg and B. Nickel, Chem. Phys. **132**, 235–242 (1989).
[63]B. Nickel and J. Hertzberg, Chem. Phys. **132**, 219–234 (1989).
[64]T. Elsaesser, F. Lärmer, W. Kaiser, B. Dick, M. Niemeyer, and W. Lüttke, Chem. Phys. **126**, 405–416 (1988).
[65]M. Meot-Ner, J. Phys. Chem. **84**, 2716–2723 (1980).
[66]P. R. van der Linde, J. G. Blok, and H. A. J. Oonk, J. Chem. Thermodyn. **30**, 909–917 (1998).
[67]I. C. E. Turcu, M. C. Gower, and P. Huntington, Opt. Commun. **134**, 66–68 (1997).
[68]R. M. Varma, D. S. Venables, A. A. Ruth, U. Heitmann, E. Schlosser, and S. Dixneuf, Appl. Opt. **48**, B159–B171 (2009).
[69]A. A. Ruth and K. T. Lynch, Phys. Chem. Chem. Phys. **10**, 7098–7108 (2008).
[70]The noble gas lines were flushed extensively before filling the chamber. The chamber was optimized for its tightness; a leak-rate of <0.2 mbar/day was established.
[71]Whether only photoproducts are required to "passivate" the walls in order to observe the dynamic loss behavior outlined here and in Ref. 24, or whether also naphthalene or both are essential, could not be conclusively determined.
[72]Indeed our goal of this work was to test, in how far multi-photon ionization of gaseous PAHs may be a viable method to replace discharges for the generation of cationic species in a selective way for CRD absorption measurements in supersonic jets (Ref. 74). In preliminary experiments, we therefore studied gaseous naphthalene as a test compound in a static cell upon exposure to a strong UV laser pulse.
[73]F. Salama and L. J. Allamandola, J. Chem. Phys. **94**, 6964–6977 (1991).
[74]L. Biennier, F. Salama, L. J. Allamandola, and J. J. Scherer, J. Chem. Phys. **118**, 7863–7872 (2003).
[75]T. Suzuki, T. Ichimura, M. Kusaba, and N. Nakashima, Chem. Phys. Lett. **263**, 197–202 (1996).
[76]A. A. Ruth, E.-K. Kim, and A. Hese, Phys. Chem. Chem. Phys. **1**, 5121–5129 (1999).
[77]T. Allain, S. Leach, and E. Sedlmayr, Astron. Astrophys. **305**, 602–615 (1996).
[78]J. H. Miller, L. Andrews, P. A. Lund, and P. N. Schatz, J. Chem. Phys. **73**, 4932–4939 (1980).
[79]K. V. Reddy, D. F. Heller, and M. J. Berry, J. Chem. Phys. **76**, 2814–2837 (1982).
[80]M. Frenklach, D. W. Clary, W. C. Gardiner, and S. E. Stein, Sym. (Int.) Combust., [Proc.] **20**, 887–901 (1985).
[81]M. Frenklach, Phys. Chem. Chem. Phys. **4**, 2028–2037 (2002).
[82]K. H. Homann, Proc. Combust. Inst. **20**, 857–870 (1985).
[83]However, in the photolysis of naphthalene C_4H_3 ions can be formed at very high energies (22 eV)[35] which could also potentially influence phase 1.
[84]The presence of molecular oxygen and/or nitrogen at levels of 1×10^{-3} mbar cannot be excluded. In the presence of oxygen, oxidation of PAH and soot particles is a process competing with processes of particle formation, inhibiting the mass of particles formed from photolysis.
[85]A similar phenomenon, due to flushing of the walls, was observed in the 1.1 dm^3 cavity where releasing helium buffer gas into the chamber resulted in an increase in loss. The particles ultimately progress out of the flow and reattach to the walls.
[86]J. Crank, *The Mathematics of Diffusion* (Clarendon, Oxford, 1975).
[87]F. P. Incropera and D. P. DeWitt, *Introduction to Heat Transfer* (Wiley, New York, 1996).
[88]*CRC Handbook of Chemistry and Physics*, 73rd ed. (CRC Press, Cleveland, 1992).
[89]T. Kunz, C. Hahn, A. Baindl, O. Nuyken, T. Lippert, F. Gassmann, and A. Wokaun, J. Phys. Chem. A **103**, 4855–4860 (1999).
[90]F. Gassmann, T. Lippert, J. Wei, and A. Wokaun, J. Phys. Chem. A **106**, 4061–4067 (2002).
[91]J. Laplante and R. Pottier, J. Phys. Chem. **86**, 4759–4766 (1982).
[92]I. R. Epstein, M. Morgan, C. Steel, and O. Valdes-Aguilera, J. Phys. Chem. **87**, 3955–3958 (1983).
[93]This suggestion was made by reviewer 1 of this publication.